

# Synthesis, characterization, and property testing of PGS/P(AMPS-co-AM) superabsorbent hydrogel initiated by glow-discharge electrolysis plasma

Jie Yu<sup>1</sup> · Haitao Zhang<sup>1</sup> · Yun Li<sup>1</sup> · Quanfang Lu<sup>1,2</sup> · Qizhao Wang<sup>1</sup> · Wu Yang<sup>1</sup>

Received: 8 June 2015 / Revised: 7 August 2015 / Accepted: 20 August 2015 / Published online: 28 September 2015  
© Springer-Verlag Berlin Heidelberg 2015

**Abstract** A palygorskite/poly(2-acrylamido-2-methyl-1-propanesulfonic acid-co-acrylamide) (PGS/P(AMPS-co-AM)) superabsorbent hydrogel was prepared in aqueous solution using glow-discharge electrolysis plasma (GDEP) as an initiator and *N,N'*-methylene-bis-acrylamide as a cross-linker. A possible copolymerization mechanism initiated by GDEP was proposed. The structure, thermal stability, and morphology of PGS/P(AMPS-co-AM) were characterized by FT-IR, XRD, TG-DTG, and SEM. The swelling kinetics, pH-reversibility, and influence of various pH and salt solutions on the swelling were investigated. Adsorption kinetics and adsorption mechanism of hydrogel for dyes were studied in detail. The results indicated that the equilibrium swelling of hydrogel is 652.6 g g<sup>-1</sup> in distilled water. The swelling of the hydrogel in salt solutions from highest to lowest is Na<sup>+</sup> > Mg<sup>2+</sup> > Fe<sup>3+</sup>. The hydrogel has pH-reversibility responsive to the pH and salts solutions. The adsorption process of dyes follows the pseudo-second-order kinetic model with multi-step diffusion process. In addition, PGS/P(AMPS-co-AM) hydrogel can be regenerated and reused.

**Keywords** Superabsorbent hydrogel · Glow-discharge electrolysis plasma (GDEP) · Palygorskite (PGS) · Graft copolymerization · Swelling behavior · Adsorption

## Introduction

Superabsorbent hydrogels are loosely cross-linked hydrophilic polymers with three-dimensional network structure which can swell without dissolving in aqueous medium, and the absorbed water is hardly lost even under some external pressure [1]. Because of containing hydrophilic groups such as –NH<sub>2</sub>, –OH, –CONH<sub>2</sub>, –COOH, and –SO<sub>3</sub>H in the network structure, most of the superabsorbent hydrogels have been responsive to environmental stimulants such as pH, ionic strength, temperature, light, and electrical field [2]. This unique feature has produced an extensive spectrum of applications in which some of them have been used in drug delivery, separation devices, hygienic products, waste water purification, agriculture, forestry, horticulture, and so on [3]. At present, it has become a research hotspot in the field of function polymer.

However, most of the superabsorbent hydrogels have been focused on synthetic polymers based on acrylic acid [4, 5]. As is known to all, these hydrogels are toxic and non-biodegradable, so they can cause serious environmental issues [1, 6]. Therefore, the development of the superabsorbent hydrogels based on eco-friendly organic/inorganic composite has attracted considerable interests. Clays, such as montmorillonite [7], attapulgite [8], vermiculite [9], and bentonite [10], have all been used for the preparation of superabsorbent hydrogel. Many studies indicated that organic monomers containing the double bond can be grafted onto the clay forming the clay-based superabsorbent hydrogel, which not only reduced the production costs, but also enhanced swelling properties,

✉ Jie Yu  
yujie741008@163.com

✉ Quanfang Lu  
luqf@nwnu.edu.cn

<sup>1</sup> Key Laboratory of Bioelectrochemistry and Environmental Analysis of Gansu Province, College of Chemistry and Chemical Engineering, Northwest Normal University, Lanzhou 730070, People's Republic of China

<sup>2</sup> Editorial Department of the University Journal, Northwest Normal University, Lanzhou 730070, People's Republic of China

mechanical performance, and thermal stability of superabsorbent hydrogels [7–10].

For improving the properties and expanding application fields, many approaches have also been utilized to synthesize superabsorbent hydrogels, such as chemical initiation [10], radiation [11], photo-curing technique [12], and so on. Recently, a novel approach for synthesis of clay-based superabsorbent hydrogels using glow-discharge electrolysis plasma (GDEP) has received great attention. For example, Gao and his co-workers successfully synthesized montmorillonite/poly(acrylic acid-co-acrylamide) [13] and montmorillonite/acrylic acid [14] superabsorbent, and optimized the reaction conditions. However, a possible initiated copolymerization mechanism and properties of the superabsorbent hydrogels prepared by GDEP have not been reported.

Glow-discharge electrolysis is a nonconventional electrochemical process in which non-thermal plasma is sustained by glow discharges between an electrode and the electrolyte around it. During GDEP, various chemical species such as  $\text{HO}\cdot$ ,  $\text{H}\cdot$ ,  $\text{HO}_2\cdot$ ,  $\text{e}_{\text{aq}}^-$ ,  $\text{H}_3\text{O}_{\text{gas}}^+$ , and  $\text{H}_2\text{O}_2$  can initiate some unusual chemical reactions [15]. In the past 20 years, this technique has been widely used for synthetic chemistry [16, 17], water purification [15, 18], oxidative degradation [19, 20], and surface modification [21, 22]. Recently, we have successfully synthesized some hydrogels by GDEP rather than chemical initiation [6, 23, 24]. The results showed that GDEP has advantages over the others, such as lower cost in setup, simple steps, and mild reaction conditions. This technique can be termed as an environment-friendly initiation, which is not requiring any additional chemicals, bubbling nitrogen and leaving some by-products [6, 24].

Palygorskite (PGS), a kind of hydrated octahedral-layered magnesium aluminum silicate mineral with reactive  $-\text{OH}$  groups on its surface, is less sensitive to salts comparing with other clays (such as smectite) [25]. So in the present work, PGS has been chosen as an excellent candidate for preparing hydrogel. Many studies have showed that increasing the number of ionic groups in the superabsorbent hydrogel is known to increase the swelling capacity, while the nonionic groups can improve the salt sensitivity of the material [8, 10]. 2-Acryloylamino-2-methyl-1-propanesulfonic acid (AMPS) is an ionic vinyl monomer including a hydrophilic sulfonic acid functional group and a nonionic amide group. Therefore, it has been introduced into hydrogels to improve the comprehensive properties by several works [26, 27]. Recently, preparing hydrogel with acrylamide (AM) as vinyl monomer has been extensively studied because AM has great advantage on its good salt-resistant performance as a raw material for hydrogel [8, 10].

In this work, a palygorskite/(2-acrylamido-2-methyl-1-propanesulfonic acid-co-acrylamide) (PGS/P(AMPS-co-AM)) superabsorbent hydrogel was prepared in aqueous solution by GDEP technique, in which *N,N'*-methylene-bis-

acrylamide (MBA) was used as a cross-linker. The structure, thermal stability, and morphology of PGS/P(AMPS-co-AM) were characterized by Fourier transform infrared spectroscopy (FT-IR), X-ray diffraction (XRD), thermogravimetric analysis (TG-DTG), and scanning electron microscopy (SEM). A possible copolymerization mechanism initiated by GDEP was proposed. The swelling behavior and the influence of various pH values and salt solutions on the equilibrium swelling were investigated in detail. Adsorption kinetics of hydrogel for cationic dyes was also studied using the pseudo-first-order model, the pseudo-second-order model, and the intra-particle diffusion model. In addition, adsorption mechanism, regeneration, and reusability of PGS/P(AMPS-co-AM) superabsorbent hydrogels for cationic dyes were also discussed.

## Experimental

### Materials

Palygorskite (PGS, Jiuchuan Nano-material Technology Co., Ltd., Jiangsu, China) was firstly treated with  $0.1 \text{ mol L}^{-1}$  HCl for 3 h, then washed with distilled water, and dried at  $105 \text{ }^\circ\text{C}$  for getting a constant weight. After that, the purified product was passed through a 100-mesh screen before use. 2-Acrylamido-2-methyl-1-propanesulfonic acid (AMPS, analytical reagent grade, Shangdong Shouguang Runde Chemical Co., Ltd., Shandong, China) was used without further purification. Acrylamide (AM, Tianjin Guangfu Fine Chemical Research Institute, Tianjin, China) was used as purchased. The cross-linker, *N,N'*-methylene-bis-acrylamide (MBA, chemical pure, Shanghai Chemical Reagent Corporation) was used as received. The two cationic dyes, crystal violet (CV) and methylene blue (MB), were supplied by Jiangsu Sopo Chemical Share-holding Co., Ltd., China. Other chemicals, such as NaOH, HCl, NaCl,  $\text{MgCl}_2$ ,  $\text{FeCl}_3$ , and ethanol, were all of analytical grade. The pH was adjusted with  $0.1 \text{ mol L}^{-1}$  solutions of HCl and NaOH.

### Synthesis of PGS/P(AMPS-co-AM) superabsorbent hydrogel

The experimental apparatus had been reported in reference [13]. The mass ratio of PGS:AMPS:AM prepared PGS/P(AMPS-co-AM) hydrogel is 0.9:4:6. In a 250-mL three-neck flask, 0.9 g PGS was placed in 25 mL distilled water. To disperse completely, the mixture was stirred for 30 min. Then, 0.07 g cross-linker MBA, 4 g AMPS, and 6 g AM were added into the mixed solution. The mixture was stirred for 20 min at  $70 \text{ }^\circ\text{C}$  until the cross-linker and monomers were dissolved completely. After that, two electrodes were inserted into the mixed solution to start the glow-discharge at 500 V for 2 min. Then, the reaction mixture was additionally stirred for

3 h. Finally, the resulting product was washed several times with methanol, dried at 60 °C. The PGS/P(AMPS-co-AM) superabsorbent hydrogel was obtained, then milled through a 100-mesh sieve for testing the properties.

### Instrumental analysis of the PGS/P(AMPS-co-AM)

Fourier transform infrared spectra (FT-IR) of the samples were recorded on a DIGILAB FTS 3000 FT-IR spectrophotometer (USA) in the range of 400–4000  $\text{cm}^{-1}$  with a KBr pellet. X-ray diffraction (XRD) of samples was obtained by a Rigaku D/max-2400 X-ray power diffractometer with  $\text{Cu-K}\alpha$  radiation ( $\lambda = 0.15406 \text{ nm}$ ), running at 40 kV and 150 mA, scanning from 5° to 80°. Thermogravimetric analysis (TG-DTG) of samples was carried out on a PE TG/DTA 6300 instrument with a nitrogen flow rate of 50  $\text{mL min}^{-1}$  and a heating rate of 10  $^{\circ}\text{C min}^{-1}$ , over a temperature range of 20–800 °C. Surface morphology of the samples was observed in JSM-6701F field emission scanning electron microscope (FE-SEM) and Zeiss Ultra Plus field emission scanning electron microscope (FE-SEM). Before SEM observation, the sample was coated with gold. Absorbance measurement of dyes was recorded on an UV757CART Ver 2.00 spectrophotometer. All pH measurements were recorded on a pH-211 Model pH meter (Hanna, Italy).

### Property testing

#### Measurements of equilibrium swelling and swelling kinetic

A series of dried samples ( $m_1$ ) were immersed in excess solution and kept swelling equilibrium. Swollen samples ( $m_2$ ) were then filtered through a 100-mesh screen for 10 min and weighted. The equilibrium swelling  $Q_{\text{eq}}$  ( $\text{g g}^{-1}$ ) was calculated as follows [24]:

$$Q_{\text{eq}} = \frac{m_2 - m_1}{m_1} \quad (1)$$

A 0.1 g dried sample was placed in 500 mL distilled water. The superabsorbent hydrogel was then separated and weighed. This process was repeated at set intervals until the weight of the swelling remained constant. The swelling  $Q_t$  at different times can be calculated according to Eq. 1.

#### Equilibrium swelling at various salt solutions and pH

The equilibrium swelling of hydrogel was determined in 0.01–0.10  $\text{mol L}^{-1}$  salt solutions ( $\text{NaCl}$ ,  $\text{MgCl}_2$ , and  $\text{FeCl}_3$ ) and various pH (1–12). Individual solutions with acidic and basic values of pH were diluted with HCl and NaOH solutions to achieve  $\text{pH} < 6.0$  and  $\text{pH} > 6.0$ , respectively. Then, 0.05 g sample was immersed entirely in 200 mL of solution and

soaked for 24 h. The equilibrium swelling was calculated according to Eq. 1.

#### Adsorption kinetic

A mixture containing 0.1 g of dried hydrogel and 200 mL of dye solution (1000  $\text{mg L}^{-1}$ ,  $\text{pH} = 5.62$ ) was shaken at 25 °C with 120  $\text{r min}^{-1}$ . The sample was taken out at the desired time-interval, then filtered and determined the absorbance by UV spectrophotometer. The adsorption capacity ( $q$ ) was calculated according to Eq. 2 [23].

$$q = \frac{(C_0 - C)V}{m} \quad (2)$$

where  $C_0$  and  $C$  ( $\text{mg L}^{-1}$ ) are the concentrations of the dyes before and after the adsorption,  $V$  (L) is the volume of the solution, and  $m$  (g) is the weight of dry hydrogel used.

#### Desorption studies

The desorption solutions were prepared with different ratios of 0.1  $\text{mol L}^{-1}$  HCl solution and ethanol. Then, the hydrogels that adsorbed CV and MB were put into desorption solutions until equilibrium. The desorption ratio ( $\eta$ ) was calculated as following:

$$\eta = 100\% \times q_2/q_1 \quad (3)$$

where  $q_2$  ( $\text{mg g}^{-1}$ ) is the release amount of dye in desorption solution and  $q_1$  ( $\text{mg g}^{-1}$ ) is the adsorption amount of dyes.

#### The regeneration and reusability experiments

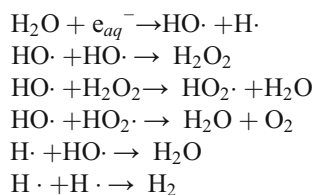
A mixture containing 0.1 g of dried hydrogel and 200 mL of dye solutions (1000  $\text{mg L}^{-1}$ ) was shaken with 120  $\text{r min}^{-1}$  for 12 h. Thereafter, the adsorbed hydrogel was placed into the optimum desorption solution (200 mL) shaking 12 h, then separated and determined the absorbance. After that, the hydrogel was washed with deionized water. Adsorption and desorption tests were repeated three times.

## Results and discussion

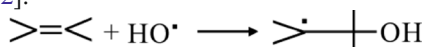
### Possible copolymerization mechanism of PGS/P(AMPS-co-AM) hydrogel initiated by GDEP

GDEP gives rise to ultraviolet light, radiation, and active species in an aqueous solution [24]. Normally, the energetic electrons produced by GDEP are about 5–20 eV [28], which can transfer energy to water molecules forming a variety of free radicals by activation, excitation,

dissociation, and ionization. The main reactions of GDEP are as follows [29]:



A highly remarkable feature of chemical results for GDEP is their strong deviation from the yield expected according to the Faraday's law [30]. Further, the products that contained species, such as radicals ( $\text{HO}\cdot$ ,  $\text{H}\cdot$ ,  $\text{HO}_2\cdot$ ), hydrated electrons ( $e_{aq}^-$ ), ions ( $\text{H}_3\text{O}_{\text{gas}}^+$ ,  $\text{OH}^-$ ), and molecules ( $\text{H}_2$ ,  $\text{H}_2\text{O}_2$ , and  $\text{O}_2$ ), are novel for normal electrolysis. The reactive species of hydroxyl radicals ( $\text{HO}\cdot$ ) and hydrogen radicals ( $\text{H}\cdot$ ) were identified using emission spectroscopic analysis by Sun et al. [31]. The  $\text{HO}\cdot$  is known to play an important role in degradation of organic compounds because it is the most powerful oxidizing species after fluorine [32]. Apart from hydrogen abstraction on labile H atoms of hydrocarbon chains (e.g.,  $\text{RH} + \text{HO}\cdot \rightarrow \text{H}_2\text{O} + \text{R}\cdot$ ),  $\text{HO}\cdot$  is able to add at double bonds [32]:



Thus, in the initiated graft copolymerization by GDEP,  $\text{HO}\cdot$  radicals produced can be introduced into the polymer chains, so the hydrogels have promising properties [6, 23, 24]. Previous studies have showed that the reaction mechanism of GDEP is similar with the chemical initiation and  $\gamma$ -ray irradiation in synthetic hydrogels process [23, 33], which is a free radical addition reaction caused by chain propagation. A possible copolymerization mechanism of PGS/P(AMPS-co-AM) initiated by GDEP is showed in Scheme 1. Initially, the water molecules absorb enough energy from plasma to form energetic species including  $\text{HO}\cdot$  and  $\text{H}\cdot$  radicals, which is termed as the free radical formation process (reaction 1). Then, apart from hydrogen abstraction on labile H atoms from the  $-\text{OH}$  of PGS,  $\text{HO}\cdot$  radicals can add at double bonds of AM and AMPS, forming the new PGS, AM, and AMPS radicals, which is called the chain initiation process (reaction 2). Thereafter, random reactions of these radicals with the AM and AMPS monomers cause the chain propagation and growth (reaction 3), so that monomers are grafted onto PGS backbone to form the graft copolymer. The degrading reaction between radicals ( $\text{H}\cdot$  and  $\text{HO}\cdot$ ) and polymer chains is ignored in this stage, owing to the formation of hydrogel to cease from further reaction if discharge time and discharge voltage are controlled appropriately [6, 24]. Meanwhile, radicals of homopolymer and copolymer of AMPS and/or AM can also be formed in reaction 3, but they do not cause appreciable unwanted

effects on the properties of the final products [24]. As a cross-linker, MBA can cross-link the polymer by reaction of its two double bonds [33]. In above stages, the homopolymer radicals, copolymer radicals, and cross-linker are coexisting, which form the cross-linked, three-dimensional network of polymer by radical-radical and cross-linking termination (Reaction 4) [6, 24, 33].

### Characterization of PGS/P(AMPS-co-AM) superabsorbent hydrogel

#### FT-IR analysis

The FT-IR spectra of PGS (a), AM (b), AMPS (c), P(AMPS-co-AM) (d), and PGS/P(AMPS-co-AM) (e) are showed in Fig. 1. It can be seen from Fig. 1a that the stretching vibration bands at 3615, 3545, and 3411  $\text{cm}^{-1}$  are assigned to  $-\text{OH}$  in Si-OH of PGS, adsorbed water, and zeolite water. The band at 1643  $\text{cm}^{-1}$  is attributed to the bending vibration of the  $-\text{OH}$  in water. The bands at 1028 and 470  $\text{cm}^{-1}$  are assigned to the stretching vibration and bending vibration of Si-O-Si in PGS [8].

In Fig. 1b, the bands at 3354 and 3184  $\text{cm}^{-1}$  are assigned to the symmetric and asymmetric stretching vibration of N-H. The bands at 1674 and 1612  $\text{cm}^{-1}$  are attributed to the stretching vibration of C=O and C=C, respectively. The bands at 1428 and 1136  $\text{cm}^{-1}$  are assigned to the deformation vibration of  $-\text{CH}_2-$  and stretching vibration of C-N in AM.

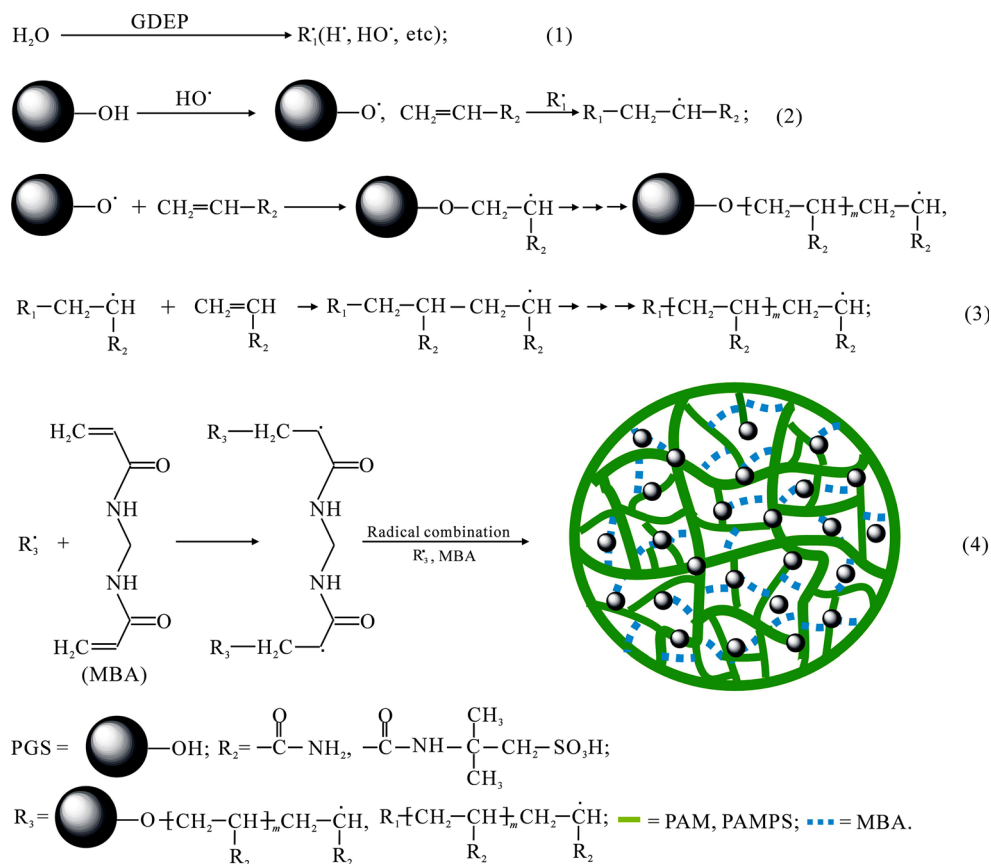
In Fig. 1c, the band at 3238  $\text{cm}^{-1}$  is assigned to the stretching vibration of N-H. The bands at 1666 and 1613  $\text{cm}^{-1}$  are assigned to the stretching vibration of C=O and C=C, respectively. The bands at 1369 and 1242  $\text{cm}^{-1}$  are assigned to the bending vibration and stretching vibration of C-N. The bands at 1086 and 626  $\text{cm}^{-1}$  are attributed to the stretching vibration of S=O and S-O, respectively [24].

It can be noticed in Fig. 1d, e that the C=C bands at 1612  $\text{cm}^{-1}$  of AM and 1613  $\text{cm}^{-1}$  of AMPS are disappeared completely. The C=O bands of AM (1674  $\text{cm}^{-1}$ ) and AMPS (1666  $\text{cm}^{-1}$ ) are strengthened and shifted to lower wavenumber (1651  $\text{cm}^{-1}$  in Fig. 1d and 1663  $\text{cm}^{-1}$  in Fig. 1e). The bands at 1111 and 1209  $\text{cm}^{-1}$  are attributed to the C-N stretching vibration of AM and AMPS, respectively. The bands at 1044 and 627  $\text{cm}^{-1}$  are assigned to the stretching vibration of S=O and S-O. This suggested that AM and AMPS had occurred copolymerization.

However, it is also observed in Fig. 1e that bands at about 3615 and 3411  $\text{cm}^{-1}$  assigned to Si-OH are almost completely disappeared. The bands at 1028  $\text{cm}^{-1}$  corresponded to the stretching of Si-O-Si is weakened and shifted to a higher wavenumber (1037  $\text{cm}^{-1}$ ), and the bands assigned to the stretching of C-N, S=O, and S-O is appeared at 1209, 1178, and 623  $\text{cm}^{-1}$ , respectively. The above information clearly indicated that AM and AMPS had been grafted onto the



**Scheme 1** Possible copolymerization mechanism of PGS/P(AMPS-co-AM) initiated by GDEP. (1) radical formation, (2) chain initiation, (3) chain propagation, (4) chain termination



OH of PGS backbone forming organic and inorganic copolymer [3, 8].

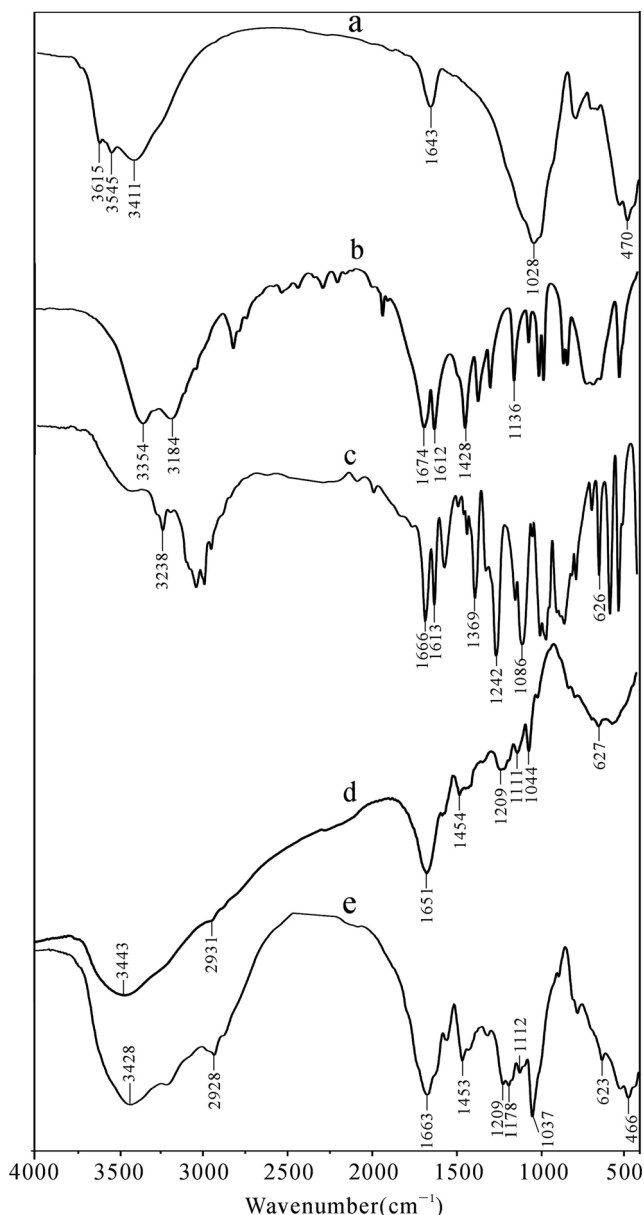
### XRD analysis

Figure 2 shows the XRD patterns of PGS (a), P(AMPS-co-AM) (b), and PGS/P(AMPS-co-AM) (c). It shows from Fig. 2a, a typical (110) diffraction peak of PGS is evident at  $2\theta = 8.04^\circ$  ( $d = 1.099$  nm). In addition, the peaks at  $2\theta = 19.60^\circ$  ( $d = 0.453$  nm),  $26.44^\circ$  ( $d = 0.337$  nm), and  $34.96^\circ$  ( $d = 0.256$  nm) are assigned to quartz and dolomite impurities [34]. In Fig. 2b, only one broad peak can be found at  $2\theta = 20.48^\circ$  ( $d = 0.433$  nm), suggesting that the P(AMPS-co-AM) is an amorphous material. After AM and AMPS monomers are grafted onto PGS by GDEP (Fig. 2c), the whole intensity of peak in the PGS/P(AMPS-co-AM) decreases sharply and the shape of the peak widens. This is because the AM and AMPS monomers are introduced to PSG forming an amorphous composite and leading to diminishing peak intensity. In addition, the lower content of PGS can also lead to decreasing the peak intensity. Further, after graft copolymer, the typical diffraction peaks and values of  $d$  are hardly unchangeable, such as the typical diffraction peak of P(AMPS-co-AM) is at  $21.64^\circ$  ( $d = 0.410$  nm) and the typical diffraction peaks of PGS are at  $8.14^\circ$  ( $d = 1.085$  nm),  $19.63^\circ$  ( $d = 0.449$  nm), and  $26.66^\circ$  ( $d = 0.334$  nm) in the PGS/

P(AMPS-co-AM), indicating that the interactions of AMPS and AM monomers during polymerization only occur on the surface of PGS without destroying the original crystallinity of the PSG [35]. Hence, it is reasonable to assume from XRD that AM and AMPS monomers have grafted onto PGS successfully by GDEP forming an amorphous composite and the graft copolymerization is hardly unchangeable the PGS crystalline.

### Thermal analysis

Thermogravimetric analysis curves of P(AMPS-co-AM) and PGS/P(AMPS-co-AM) are depicted in Fig. 3. It is obvious from TG (Fig. 3a) that the thermal stability of the PGS/P(AMPS-co-AM) is increased after grafting AMPS and AM onto PGS as compared with the P(AMPS-co-AM). Both the P(AMPS-co-AM) and PGS/P(AMPS-co-AM) exhibited four-step continuous thermal decomposition with increase in temperature. Weight losses of 3.0 % from 25 to 198 °C of P(AMPS-co-AM) and PGS/P(AMPS-co-AM) are ascribed to the removal of absorbed and bonded water. The second weight losses of 35.1 % for P(AMPS-co-AM) and 28.6 % for PGS/P(AMPS-co-AM) from 198 to 346 °C can be attributed to decomposition of low polymer and removal of the hydroxide groups, imide, and amine groups [36, 37]. The third weight losses about 17.8 % for P(AMPS-co-AM) and 19.3 %



**Fig. 1** FT-IR spectra of PGS (a), AM (b), AMPS (c) and PGS/P(AMPS-co-AM) (d)

for PGS/P(AMPS-co-AM) from 346 to 468 °C are ascribed to the loss of sulfonic groups and the destruction of cross-linked network structure [37, 38]. The fourth weight losses about 39.0 % for P(AMPS-co-AM) and 7.8 % for PGS/P(AMPS-co-AM) from 468 to 796 °C are ascribed to the breakage of main chains in polymeric backbone. The total weight losses of P(AMPS-co-AM) and PGS/P(AMPS-co-AM) are 94.9 % and 58.7 % at about 800 °C. All results suggested that the introduction of PGS into P(AMPS-co-AM) can increase the thermal stability [36, 38].

In order to further prove the result that PGS/P(AMPS-co-AM) is more stability than P(AMPS-co-AM), the DTG curves are showed in Fig. 3b. As can be seen from Fig. 3b, the maximum temperature ( $T_{max}$ ) of characteristic endothermic peak is

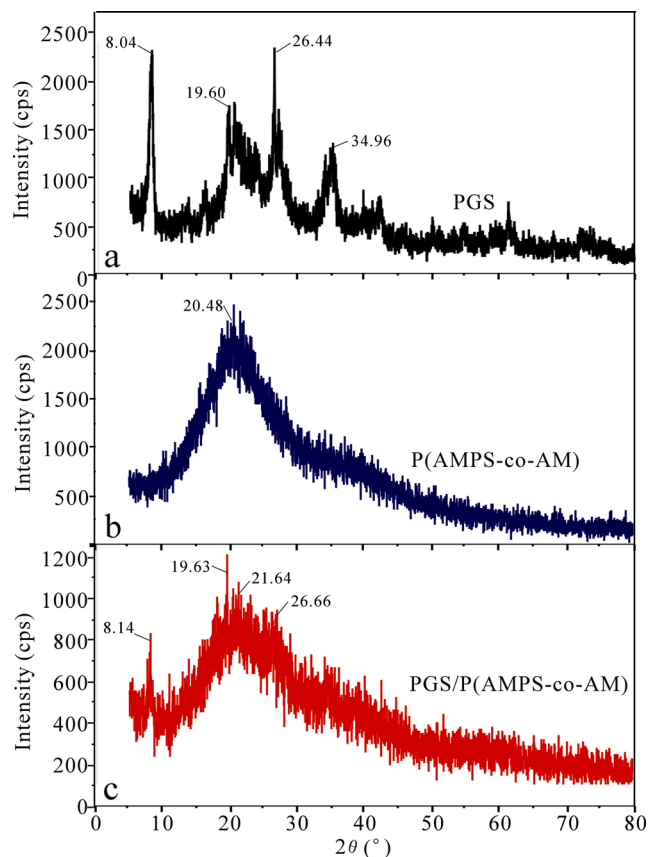


**Fig. 2** XRD of PGS (a), P(AMPS-co-AM) (b), and PGS/P(AMPS-co-AM) (c)

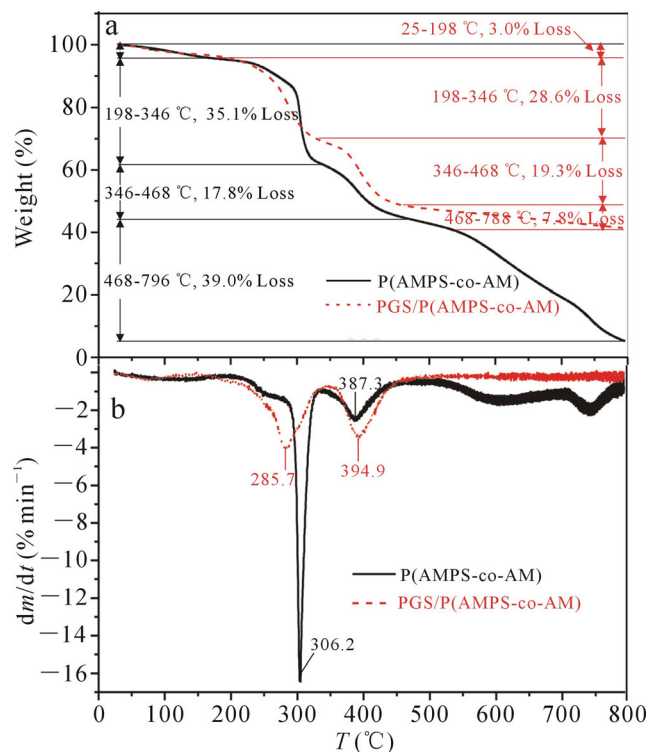


**Fig. 3** The TG (a) and DTG (b) curves of P(AMPS-co-AM) and PGS/P(AMPS-co-AM)

shifted from 387.3 °C (P(AMPS-co-AM)) to 394.9 °C (PGS/P(AMPS-co-AM)) after introduction of PGS to copolymerization. That is to say, the PGS/P(AMPS-co-AM) exhibits slower weight loss and thermal decomposition rate, revealing the grafted AMPS and AM into PGS can improve the thermal stability of the PGS/P(AMPS-co-AM) [1, 38].

### Morphological analysis

The micrographs of PGS, P(AMPS-co-AM), and PGS/P(AMPS-co-AM) at different magnifications are showed in Fig. 4. As can be seen from Fig. 4 a–a<sub>2</sub>, the PGS shows individual nanorods. The size and length of the nanorods are about 40–60 and 400–800 nm, respectively. The micrographs of P(AMPS-co-AM) (Fig. 4 b–b<sub>2</sub>) and PGS/P(AMPS-co-AM) (Fig. 4 c–c<sub>2</sub>) exhibit a rough surface morphology with visible wrinkles and three-dimensional porous structure. The diameter of micro-pores for P(AMPS-co-AM) and PGS/P(AMPS-co-AM) are about 2 μm (Fig. 4 b<sub>1</sub> and b<sub>2</sub>) and 5 μm (Fig. 4 c<sub>1</sub> and c<sub>2</sub>), respectively. That is to say, the micro-pores of PGS/P(AMPS-co-AM) are bigger than that of P(AMPS-co-AM), which causes a larger surface area of PGS/P(AMPS-co-AM) compared with P(AMPS-co-AM). In addition, the PGS nanorods are dispersed well in PGS/P(AMPS-co-AM), and the interface between the P(AMPS-co-AM) and PGS is not very clear. This means that AMPS, AM, and PGS combine very well. This unique structure can increase the area of contact

with the water effectively, facilitate water molecules and dye molecules to diffuse into the polymeric network, accelerate the swelling rate and adsorption rate, and improve water absorbency and adsorption capacities of hydrogel [38–40].

### Properties testing

To study the properties of hydrogel, five dried hydrogels (0.1 g) were placed in distilled water, 0.05 mol L<sup>-1</sup> salt solution (NaCl and FeCl<sub>3</sub>) and 1000 mg L<sup>-1</sup> dye solution (CV and MB), respectively, and allowed to equilibrate for 12 h. Figure 5 shows the changes of shape and color of PGS/P(AMPS-co-AM). Before swelling (a), the dry gel is off-white in color and too hard, but after 12 h in distilled water, it becomes very soft, larger, and colorless (Fig. 5b). This is because the ionic units presented in the PGS/P(AMPS-co-AM) hydrogel create an osmotic pressure difference between the network and the swelling medium [24]. Large amounts of water diffuse into the network to balance the osmotic pressure difference, resulting in the swelling of hydrogel. The equilibrium swelling of PGS/P(AMPS-co-AM) hydrogel in distilled water is 652.6 g g<sup>-1</sup>. In NaCl solution (Fig. 5c), the hydrogel absorbs some water and occurs to swelling and the maximum swelling is 69 g g<sup>-1</sup>. However, after the dry hydrogels were immersed into FeCl<sub>3</sub>, CV, and MB solutions, both the color and shape of samples were changed. The hydrogel samples become bulgy due to the slight swelling and brown (in FeCl<sub>3</sub>

**Fig. 4** SEM micrographs of PGS (a ×5000, a<sub>1</sub> ×10,000, a<sub>2</sub> ×50,000), P(AMPS-co-AM) (b ×1000, b<sub>1</sub> ×5000, b<sub>2</sub> ×10,000), and PGS/P(AMPS-co-AM) (c ×1000, c<sub>1</sub> ×5000, c<sub>2</sub> ×10,000) at different magnifications

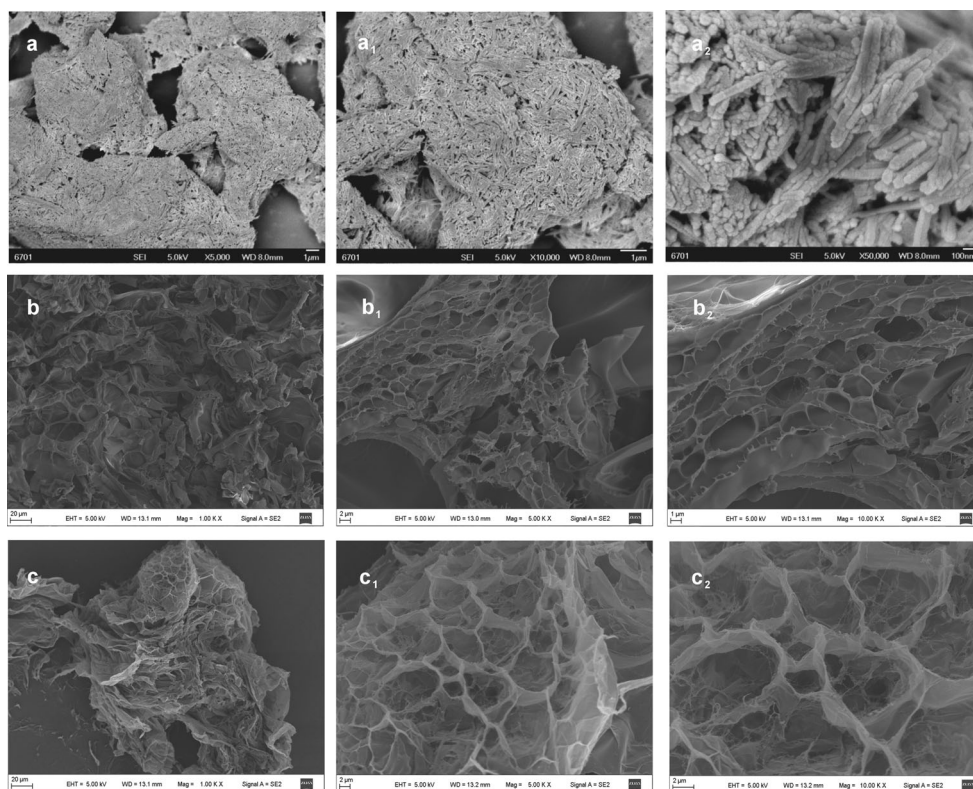
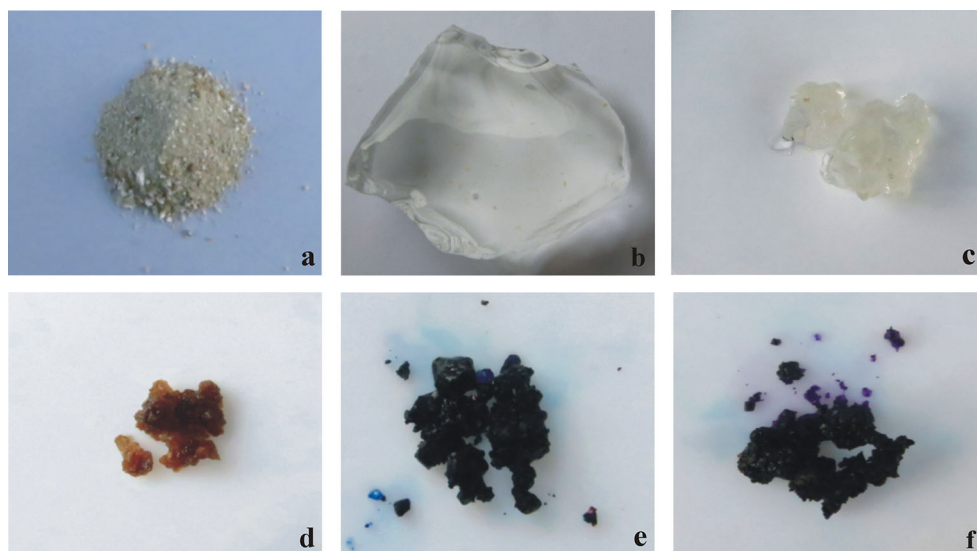


**Fig. 5** Photographs of dry hydrogel (a), swelling in distilled water (b), swelling in NaCl (c) and FeCl<sub>3</sub> (d), and adsorption of MB (e) and CV (f)



solution) (Fig. 5d), violet (in CV solution) (Fig. 5e), or blue (in MB solution) (Fig. 5f). This phenomenon further confirmed that the PGS/P(AMPS-co-AM) hydrogel prepared by GDEP is able to absorb some metal ions and cationic dyes from aqueous solutions.

#### Swelling behavior

In practical versatility as superabsorbent hydrogel especially for agricultural application, not only a higher swelling is required but also a higher swelling rate is needed. To investigate their swelling properties, the hydrogel samples were left in distilled water, yellow river water, and top water and their swelling were determined at consecutive time intervals. Changes in swelling with time are given in Fig. 6. Initially, the swelling increased sharply within 30 min, then began slowly, and took 60 min to reach equilibrium state, implying that PGS/P(AMPS-co-AM) hydrogel has fast swelling rate. The equilibrium swelling of PGS/P(AMPS-co-AM) in distilled water, yellow river water, and top water are 652.6, 171.8, and 175.4 g g<sup>-1</sup>, respectively. The equilibrium swelling of PGS/P(AMPS-co-AM) in distilled water is higher than that

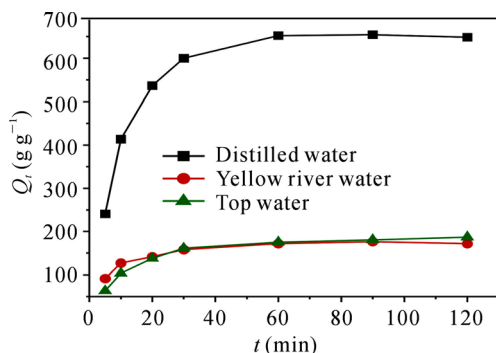


**Fig. 6** Swelling behavior of the PGS/P(AMPS-co-AM) in different solutions

of yellow river water and top water. Because there are lots of metal ions, such as K<sup>+</sup>, Na<sup>+</sup>, Mg<sup>2+</sup>, Ca<sup>2+</sup>, and Fe<sup>3+</sup> in yellow river water and top water, which diffuse into the hydrogel network, resulting in the formation of chemical cross-linking and “charge screening effect” [24].

For swelling of hydrogel, pseudo-second-order kinetics model can be used to evaluate the characteristics of swelling curves and is showed below [41, 42]:

$$\frac{t}{Q_t} = A + Bt \quad (4)$$

where  $Q_t$  (g g<sup>-1</sup>) is the swelling at time  $t$  (min).

$$A = \frac{1}{k_s Q_e^2} \quad (5)$$

$$B = \frac{1}{Q_e} \quad (6)$$

$A$  is an initial swelling rate  $[(dQ/dt)_0]$  of the hydrogel,  $k_s$  (g g<sup>-1</sup> min<sup>-1</sup>) is a constant rate for swelling, and  $Q_e$  (g g<sup>-1</sup>) is a theoretical swelling value at equilibrium.  $Q_e$  and  $k_s$  are calculated by linear fitting of  $t/Q_t$  against  $t$  showed in Fig. 7 to

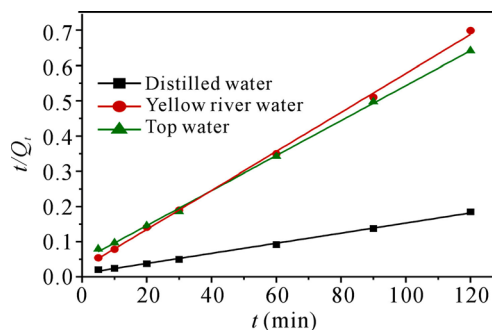


**Fig. 7** Swelling rate curves of PGS/P(AMPS-co-AM) in different solutions



**Table 1** Parameters of the swelling kinetic at different solution

	$Q_{ex}$ (g g <sup>-1</sup> )	$Q_e$ (g g <sup>-1</sup> )	$k_s(\times 10^{-4}$ g g <sup>-1</sup> min <sup>-1</sup> )	$k_{is}$ (g g <sup>-1</sup> min <sup>-1</sup> )	$R^2$
The distilled water	652.6	694.4	2.23	95.06	0.9975
The yellow river	171.8	180.8	12.52	36.96	0.9988
The top water	175.4	201.6	5.27	16.22	0.9992

Eqs. 4–6. The initial swelling rate  $k_{is}$  (g g<sup>-1</sup> min<sup>-1</sup>) is calculated as the following [42]:

$$k_{is} = k_s Q_{ex}^2 \quad (7)$$

where  $Q_{ex}$  (g g<sup>-1</sup>) is experimental equilibrium swelling. The values associated to parameters of Eqs. 4–7 are presented in Table 1. As can be seen from Fig. 7 and Table 1, the pseudo-second-order kinetic model fits well the experimental data, and the correlation coefficient ( $R^2$ ) is close to 1.

#### Effect of pH on the equilibrium swelling

The equilibrium swelling of ionic superabsorbent hydrogels is different at changing pH solutions. As the equilibrium swelling of all “anionic” hydrogels is greatly influenced by ionic strength, no buffer solutions were used [38]. Figure 8 shows the effect of pH on the equilibrium swelling of the superabsorbent hydrogel. As can be seen from Fig. 8, the equilibrium swelling of PGS/P(AMPS-co-AM) is lower at pH < 4 or pH > 9 solutions. However, the higher equilibrium swelling of the hydrogel is at pH = 4–9 solution. Under acidic pH (pH < 4), most of the  $-\text{SO}_3^-$  are protonated forming  $-\text{SO}_3\text{H}$ . On the one hand, the hydrogen-bonding interaction among  $-\text{NH}_2$ ,  $-\text{OH}$ , and  $-\text{SO}_3\text{H}$  groups is strengthened and the physical cross-linking is generated; on the other hand, the anion-anion electrostatic repulsion is restricted, consequently, the osmotic pressure of inside the hydrogel particles is decreased [36, 38]. So the network tends to shrink and collapse, and consequently, equilibrium swelling is decreased. At higher

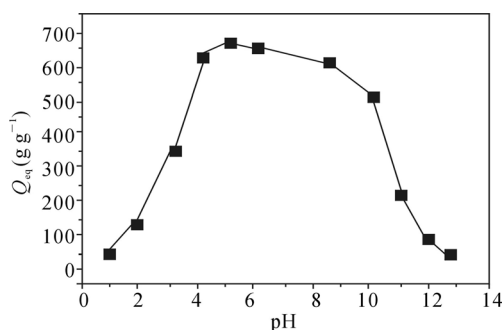


**Fig. 8** Effect of pH on the equilibrium swelling of PGS/P(AMPS-co-AM)

pHs (4–9), on the one hand, the hydrogen-bonding interaction is broken, some of the  $-\text{SO}_3\text{H}$  groups are deprotonated and ionized to a negatively charged  $-\text{SO}_3^-$ , which cause high anion-anion repulsion and high swelling capacity [38]. Also, increasing the anion density in the hydrogel can enhance the osmotic pressure inside the hydrogel. The osmotic pressure difference between the internal and external particles is balanced by the swelling of the hydrogel. As a result, the equilibrium swelling is higher and hardly changes within pHs (4–9). However, at higher pH (pH > 9), the equilibrium swelling is decreased due to the “charge screening effect” of excess  $\text{Na}^+$  in the swelling media (NaOH solution), which not only prevents effective anion-anion repulsion but also shields the  $-\text{SO}_3^-$  [38, 43]. So the ionic strength of the medium is increased, and consequently the equilibrium swelling is decreased.

#### Effect of salt solution on the equilibrium swelling

The ionic strength affects the equilibrium swelling of superabsorbent hydrogels [42, 43]. Figure 9 shows that the equilibrium swelling of hydrogels decreases in NaCl,  $\text{MgCl}_2$ , and  $\text{FeCl}_3$  (0.01–0.10 mol L<sup>-1</sup>) solution with the concentration of the salt solution increased. The reason of the phenomenon is that the osmotic pressure difference between the hydrogel and the external solution is decreased with the increase of the salt concentration by the charge screening effect of the cations, which prevents the perfect anion-anion repulsive forces. As can be seen from Fig. 9 the equilibrium swelling of the hydrogel from highest to lowest is  $\text{Na}^+ > \text{Mg}^{2+} > \text{Fe}^{3+}$  in the same concentration. This is because  $\text{Mg}^{2+}$  and  $\text{Fe}^{3+}$  can form inter- and intramolecular complexes with  $-\text{NH}_2$ ,  $-\text{SO}_3\text{H}$ , and  $-\text{OH}$  in hydrogels, leading to deswelling or contraction [27, 43]. An additional reason may be the increased electrostatic attraction between anionic sites of chains and multi-valent ( $\text{Mg}^{2+}$  and  $\text{Fe}^{3+}$ ) cations resulting in an increase in the “ionic cross-linking” degree of hydrogel, which lead to it more rigid and subsequent loss of swelling [27, 44].

#### pH-Reversibility of PGS/P(AMPS-co-AM)

As the PGS/P(AMPS-co-AM) superabsorbent hydrogel shows different swelling behaviors at different pH solutions, so pH-reversibility behavior is determined at pH 6.5 and 2.0.

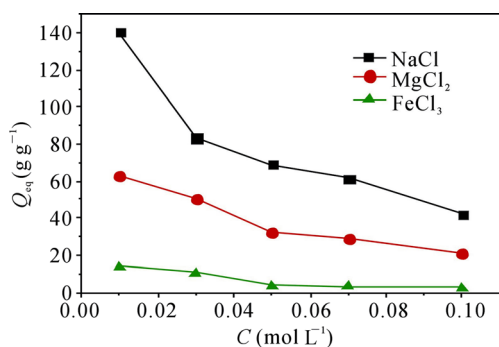


**Fig. 9** Equilibrium swelling of the PGS/P(AMPS-co-AM) in different salt solutions

In Fig. 10, a stepwise reproducible swelling-deswelling change of the hydrogel is showed at 25 °C between pH = 6.5 and pH = 2.0. At pH 6.5, the anion-anion electrostatic repulsion gives rise to the swelling of the hydrogel, while at pH 2.0, it shrinks due to protonation of  $-\text{SO}_3^-$  and hydrogen-bonding interaction among  $-\text{NH}_2$ ,  $-\text{SO}_3\text{H}$ , and  $-\text{OH}$  [26, 43]. After six swelling-deswelling cycles, the hydrogel still has a better response to environmental pH stimulants, indicating that the PGS/P(AMPS-co-AM) has excellent pH reversibility. In addition, it can be seen from Fig. 10 that there is a certain decreased trend after every time of swelling-deswelling. Repeated six times, the maximum equilibrium swelling of hydrogel in pH 6.5 is about  $366 \text{ g g}^{-1}$ . The deviation may be a quality loss when we collected the hydrogel in every time. Even so, it is also preliminarily indicated that the hydrogel has pH-reversibility.

#### Adsorption kinetics of dyes

As can be seen from Fig. 5, PGS/P(AMPS-co-AM) superabsorbent hydrogel not only exhibits water absorbency but also has adsorption of dyes. Therefore, it is expected that the hydrogel can be also used for waste water purification. Figure 11 shows the adsorption of PGS/P(AMPS-co-AM) for MB and CV dyes at consecutive time intervals. Initially, the adsorptions of hydrogel for CV and MB increase sharply within

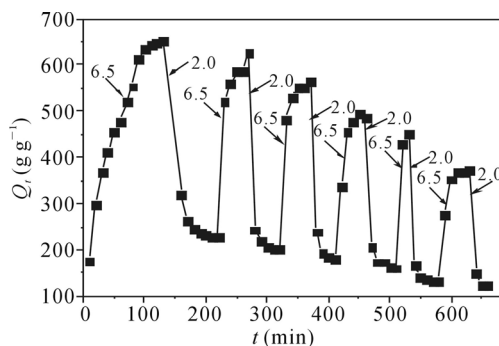


**Fig. 10** pH-reversibility of PGS/P(AMPS-co-AM) between pH = 6.5 and pH = 2.0

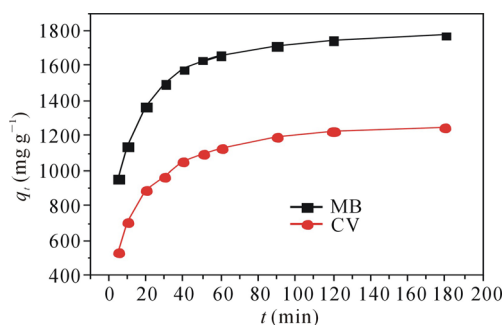


**Fig. 11** Kinetics of adsorption capacity of MB and CV by PGS/P(AMPS-co-AM)

60 min, then begin to slowly, and finally level off after 2 h, implying that PGS/P(AMPS-co-AM) hydrogel has a fast adsorption rate.

In order to investigate the mechanism and rate-controlling step in the overall adsorption process, the pseudo-first-order kinetics model, the pseudo-second-order kinetics model, and the intra-particle diffusion model were used to test experimental data [45].

The pseudo-first-order kinetic model is as follows:

$$\log(q_e - q_t) = \log q_e - \frac{k_1}{2.303} t \quad (8)$$

where  $q_e$  and  $q_t$  ( $\text{mg g}^{-1}$ ) are the amounts of dyes adsorbed on the adsorbent at equilibrium and at any time  $t$  (min), and  $k_1$  ( $\text{min}^{-1}$ ) is the rate constant of the pseudo-first-order adsorption. The value of the adsorption rate constant  $k_1$  and

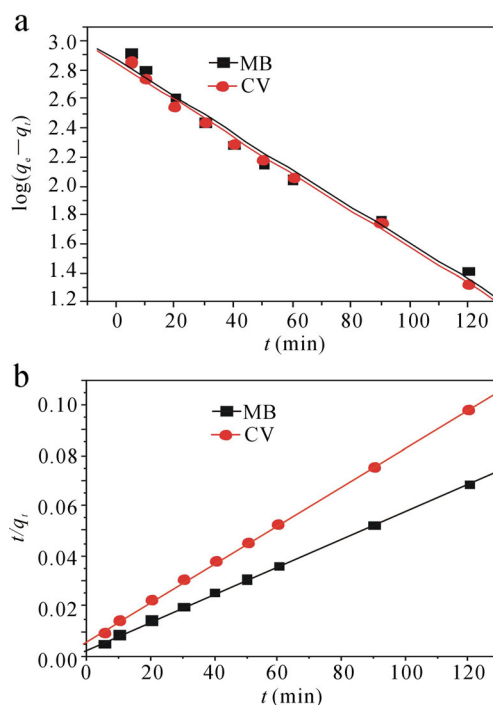


**Fig. 12** Pseudo-first-order kinetics (a) and pseudo-second-order kinetics (b) for adsorption of MB and CV on PGS/P(AMPS-co-AM)

**Table 2** Kinetic parameters for the adsorption of cationic dyes on PGS/P(AMPS-co-AM)

Dye	$q_e$ (exp) (mg g <sup>-1</sup> )	Pseudo-first-order model			Pseudo-second-order model		
		$k_1$ (min <sup>-1</sup> )	$q_e$ (mg g <sup>-1</sup> )	$R^2$	$k_2$ (g mg <sup>-1</sup> min <sup>-1</sup> )	$q_e$ (mg g <sup>-1</sup> )	$R^2$
MB	1772.1	0.0290	735.0	0.9892	$9.10 \times 10^{-5}$	1827.9	0.9999
CV	1246.4	0.0291	695.2	0.9963	$8.31 \times 10^{-5}$	1310.0	0.9997

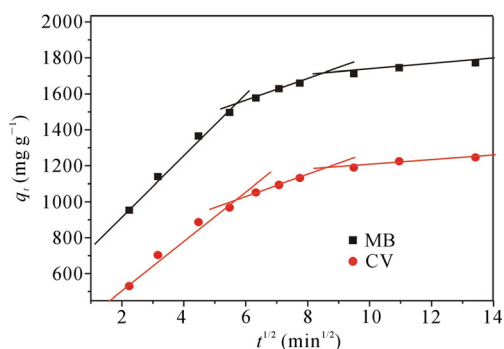
theoretical equilibrium amount of  $q_e$  can be obtained from the slope and intercept of the straight-line plots of  $\log(q_e - q_t)$  against  $t$ . The pseudo-first-order kinetics model assumes that the adsorption is originated from physical process. In many cases, the pseudo-first-order kinetic model is generally applicable over the initial stage of the adsorption processes [46].

The pseudo-second-order kinetics model is expressed as follows:

$$\frac{t}{q_t} = \frac{1}{k_2 q_e^2} + \frac{t}{q_e} \quad (9)$$

where  $k_2$  (g mg<sup>-1</sup> min<sup>-1</sup>) is the rate constant of the pseudo-second-order equation. The values of  $k_2$  and  $q_e$  can be obtained from the slope and intercept of the plot of  $t/q_t$  against  $t$ . The pseudo-second-order kinetics model is more likely to predict the behavior over the whole range of adsorption processes and is in agreement with the chemisorption mechanism being the rate-controlling step [47].

Figure 12 shows the curve-fitting plots of the pseudo-first-order and pseudo-second-order models. By comparing Fig. 12a, b, it is obvious that pseudo-second-order kinetics model agrees with the experimental data better than the pseudo-first-order model. The kinetic parameters for the adsorption of cationic dyes on PGS/P(AMPS-co-AM) are showed in Table 2. As can be seen from Table 2, the correlation coefficient  $R^2$  of the pseudo-second-order adsorption model is higher than that of the pseudo-first-order kinetics; moreover, the calculated  $q_e$  values obtained from the pseudo-second-order kinetics model are closer to the experimental  $q_e$ (exp) than that from the pseudo-first-order kinetics.

**Fig. 13** Intra-particle diffusion kinetic for adsorption of MB and CV on PGS/(AMPS-co-AM)

These results suggest that the pseudo-second-order adsorption mechanism is predominant, and the rate-limiting step in the adsorption process of two dyes onto PGS/P(AMPS-co-AM) may be a chemisorption process involving valence forces through sharing or exchange of electrons between the dyes and the adsorbent.

Weber's diffusion model is the most commonly used technique for identifying the adsorption mechanism of porous materials. Weber's diffusion model is expressed as [46]:

$$q_t = k_{\text{int}} t^{1/2} + I \quad (10)$$

where  $I$  is the intercept which obtains an idea thickness of the boundary layer on the adsorbent surface and  $k_{\text{int}}$  (mg g<sup>-1</sup> min<sup>-1/2</sup>) is the intraparticle diffusion rate constant. Generally, if the intraparticle diffusion is the only rate-controlling step, then the plot passes through the origin; if not, the boundary layer diffusion affects the adsorption to some extent [46, 47].

Figure 13 shows that the adsorption plots of  $q_t$  versus  $t^{1/2}$  are not linear over the whole time range and can be separated into three linear sections with different slopes, which indicated that two or more steps occur in the adsorption process. The first portion can be attributed to the diffusion of adsorbate through the solution to the external surface of adsorbent or the boundary layer diffusion of solute molecules, where the adsorption rate is high. The second portion illustrates the gradual adsorption stage, where intra-particle diffusion rate is rate-controlling. The third portion refers to the final equilibrium stage in which the intra-particle diffusions start to slow and level out [47, 48]. It can be also observed from Fig. 13 that the plots do not pass through the origin ( $I \neq 0$ ); this is indicative of

**Table 3** Comparison of adsorption capacities (mg g<sup>-1</sup>) for cationic dyes of different hydrogel produced by other techniques

Adsorbent	Preparation techniques	Adsorption capacity (mg g <sup>-1</sup> )		Reference
		CV	MB	
PGS/P(AMPS-co-AM)	GDEP	1246.4	1772.1	This work
P(DMAM-co-ANa)	Chemical initiator	320.0	800.0	[2]
P(AA-AM)	Chemical initiator	40.3	45.8	[4]
P(AAm/AAcNa)	Irradiation	103.2	–	[5]
CTS-g-PAA/VMT	Chemical initiator	–	1685.6	[9]

**Table 4** The desorption capacity ( $\text{mg g}^{-1}$ ) and desorption ratio (%) of hydrogel in different solution

$V_{\text{ethanol}}:V_{\text{HCl}}$	MB desorption capacity ( $\text{mg g}^{-1}$ )	MB desorption ratio (%)	CV desorption capacity ( $\text{mg g}^{-1}$ )	CV desorption ratio (%)
100:0	36.56	2.25	1.24	0.12
80:20	658.30	40.60	594.57	49.50
60:40	693.26	42.76	859.60	72.39
50:50	666.67	41.12	910.08	76.01
40:60	784.74	48.40	746.66	62.20
20:80	587.22	36.22	842.52	70.21
0:100	341.99	21.09	717.53	59.80

some degree of boundary layer control and this further shows that the intraparticle diffusion is not the only rate-limiting step, but other processes may control the rate of adsorption simultaneously [49]. Similar results were reported in adsorption of Congo Red on coal-based mesoporous activated carbon [47] and adsorption of ginsenosides on polymeric resins [48].

The comparison of adsorption capacity of MB and CV onto various adsorbents obtained by other techniques was listed in Table 3. It shows that the PGS/P(AMPS-co-AM) has a very large adsorption capacity. This suggests that the PGS/P(AMPS-co-AM) can be considered a promising adsorbent for the adsorption of CV and MB from aqueous solutions. In addition, the higher adsorption capacities indicate once again that the GEDP technique has advantages over the others, which can be applied to initiate the polymerization reaction as a rich source of free radicals in aqueous solution.

#### Desorption and reusability of PGS/P(AMPS-co-AM) superabsorbent hydrogels

To check the economic feasibility, desorption studies were also carried out. The desorption capacity and desorption ratio were listed in Table 4. As can be seen from Table 4, the desorption ratio is low at  $0.1 \text{ mol L}^{-1}$  HCl or ethanol. However, the desorption ratios is higher at mixture solution of HCl and ethanol. The best desorption conditions ( $V_{\text{HCl}}:V_{\text{ethanol}}$ ) of MB and CV are 40:60 and 50:50, and desorption ratios are 48.40 % and 76.01 %, respectively. This is

because most of the  $-\text{SO}_3^-$  groups in PGS/P(AMPS-co-AM) hydrogel are protonated forming  $-\text{SO}_3\text{H}$  under acid condition and the electrostatic interaction between  $-\text{SO}_3^-$  group and cationic dye is restricted. In addition, the network of hydrogel tends to shrink and collapse under acid condition, and consequently, equilibrium adsorption is decreased. The desorption capacity of MB is lower than that of CV because of different structure.

The reusability of the adsorbent material is likely to be one of the most important features related to the application potential of adsorption technology. Therefore, the adsorption-desorption property of hydrogel was tested under the optimum desorption condition, and the results were showed in Table 5. After three adsorption-desorption experiments, the desorption ratios of MB and CV are 53.90 % and 68.22 %. The reusability of PGS/P(AMPS-co-AM) superabsorbent hydrogel is not ideal; even so, the results also indicate that the hydrogel has certain desorption behavior and regeneration.

#### Proposed adsorption mechanism

Many studies have discussed the adsorption mechanism of dye to hydrogel [50–53]. Interaction between the dye and hydrogel are mainly swelling, van der Waals, hydrophobic interaction, electrostatic interaction, and hydrogen bonding [50, 52]. Among these forces, hydrophobic interactions and van der Waals have been commonly recognized as hydrogel adsorbents [50, 53]. In this study, adsorption occurs mainly through the  $-\text{SO}_3\text{H}$  and  $-\text{OH}$  as the hydrogels having these groups have high affinities for cationic dyes.

In the case of neutral solution, the PGS/P(AMPS-co-AM) hydroge ( $\text{OH}-\bullet-\text{SO}_3\text{H}$ ) were dissociated.



So, hydroge absorbs some water and occurs swelling due to the osmotic pressure difference.

Also, the cationic dyes ( $\text{RNCl}$ ) are dissolved, dissociated, and converted to cationic dye ions ( $\text{NR}^+$ ).



Then, higher swelling of hydrogel allows dye molecules to diffuse into the network structure. The adsorption process is

**Table 5** Adsorption capacity ( $\text{mg g}^{-1}$ ), desorption capacity ( $\text{mg g}^{-1}$ ), and desorption ratio (%) of consecutive three adsorption-desorption cycles

Dye	First			Second			Third		
	$q_1$ ( $\text{mg g}^{-1}$ )	$q_2$ ( $\text{mg g}^{-1}$ )	$\eta$ (%)	$q_1$ ( $\text{mg g}^{-1}$ )	$q_2$ ( $\text{mg g}^{-1}$ )	$\eta$ (%)	$q_1$ ( $\text{mg g}^{-1}$ )	$q_2$ ( $\text{mg g}^{-1}$ )	$\eta$ (%)
MB	1697.28	718.21	42.32	1337.69	655.11	48.97	1165.26	628.08	53.90
CV	1134.72	925.72	81.56	1055.75	800.26	75.80	989.95	675.35	68.22

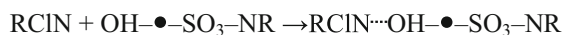
$q_1$  ( $\text{mg g}^{-1}$ ),  $q_2$  ( $\text{mg g}^{-1}$ ), and  $\eta$  (%) are the adsorption amount of dyes, the release amount of dye in desorption solution, and the desorption ratio, respectively



due to the electrostatic attraction between these two counter ions:



In addition, hydrogel prepared by GDEP technique possesses abundant hydroxyl groups (–OH) which can form hydrogen bonding with amino groups of the dyes (RNCl).



All above interactions between hydrogel and dye molecules lead to the high adsorption capacity of the hydrogel. A similar result was reported previously by Reddy and Lee for the adsorption of dyes on magnetic chitosan composites [51].

Kinetic studies indicated that the adsorption follows a pseudo-second-order kinetic model, suggesting the chemisorption is the rate-limiting step. The intraparticle diffusion is not the dominating adsorption mechanism, so the adsorption mechanism is a multistep complex process. The difference in the adsorption capacity of CV and MB may mainly be attributed to the chemical structure, size of dye molecules and the solubility of each dye [50, 53].

## Conclusion

As a promising approach, GDEP technique can initiate successfully synthesis of PGS/P(AMPS-co-AM) superabsorbent hydrogel with high performance. Compared with other initiation techniques, the GDEP technique used in this work has the advantage to be environmentally friendly since the reactive species are created without requiring any additional reagents and leaving some unwanted residues. Furthermore, HO· radicals generated by GDEP in aqueous solutions can be added to the polymer chains, so the superabsorbent hydrogel has better properties. FT-IR and XRD indicated that AMPS and AM have successfully grafted to the PGS backbone. TG-DTG indicated that the PGS/P(AMPS-co-AM) superabsorbent hydrogel has a higher thermal stability. SEM showed that the PGS/P(AMPS-co-AM) superabsorbent hydrogel exhibits a rough and porous structure with visible wrinkles. The equilibrium swelling of PGS/P(AMPS-co-AM) superabsorbent hydrogel in distilled water is  $652.6 \text{ g g}^{-1}$ . The PGS/P(AMPS-co-AM) superabsorbent hydrogel shows high pH-sensitivity, salt-sensitivity, and pH-reversibility. The adsorption process of dyes follows a pseudo-second-order kinetic model with multi-step diffusion process and the maximum adsorption capacities found for MB and CV are 1772.1 and 1246.4  $\text{mg g}^{-1}$ , respectively. In addition, the PGS/P(AMPS-co-AM) superabsorbent hydrogel has certain regeneration and reusability. All those results suggested that GDEP may provide a new approach for the preparation of clay-based hydrogels. PGS/P(AMPS-

co-AM) superabsorbent hydrogel has excellent water absorbency, pH-sensitivity, salt-sensitivity, and promising absorption properties, which can be considered as a very promising candidate for hygiene products, agriculture, horticulture, and waste water purification.

**Acknowledgments** This work was supported in part by National Natural Science Foundation of China (no. 21367023), Natural Science Foundation of Gansu Province (nos. 1308RJZA144 and 1208RJZA161), Scientific Research Project in Higher Education Institutions of Gansu Province (no. 2013-019), and Key Project of Young Teachers' Scientific Research Promotion of Northwest Normal University (no. NWNLU-LKQN-12-9), China.

## References

- Zheng Y, Gao TP, Wang AQ (2008) Preparation, swelling, and slow-release characteristics of superabsorbent composite containing sodium humate. *Ind Eng Chem Res* 47:1766–1773
- Massoud A, Waly SA (2014) Preparation and characterization of poly (acrylic acid-dimethylaminoethylmethacrylate) as amphoteric exchange resin and its adsorption properties. *Colloid Polym Sci* 292:3077–3083
- Appel EA, del Barrio J, Loh XJ, Scherman OA (2012) Supramolecular polymeric hydrogels. *Chem Soc Rev* 41: 6195–6214
- Li SF, Zhang H, Feng JT, Xu R, Liu XL (2011) Facile preparation of poly(acrylic acid-acrylamide) hydrogels by frontal polymerization and their use in removal of cationic dyes from aqueous solution. *Desalination* 280:95–102
- Ismail LFM, Maziad NA, Abo-Farha SA (2005) Factors affecting the adsorption of cationic dyes on polymeric hydrogels prepared by gamma irradiation. *Polym Int* 54:58–64
- Yu J, Yang GG, Li Y, Yang W, Gao JZ, Lu QF (2013) Synthesis, characterization, and swelling behaviors of acrylic acid/ carboxymethyl cellulose superabsorbent hydrogel by glow-discharge electrolysis plasma. *Polym Eng Sci* 54:2310–2320
- Kabiri K, Zohuriaan-Mehr MJ (2004) Porous superabsorbent hydrogel composites: synthesis, morphology and swelling rate. *Macromol Mater Eng* 289:653–661
- Zhang JP, Chen H, Wang AQ (2006) Study on superabsorbent composite. IV. Effects of organification degree of attapulgit on swelling behaviors of polyacrylamide/organo-attapulgit composites. *Eur Polym J* 42:101–108
- Liu Y, Zheng Y, Wang AQ (2010) Enhanced adsorption of methylene blue from aqueous solution by chitosan-g-poly(acrylic acid)/ vermiculite hydrogel composites. *J Environ Sci-China* 22:486–493
- Wu J, Lin J, Zhou M, Wei C (2000) Synthesis and properties of starch-graft-polyacrylamide/clay superabsorbent composite. *Macromol Rapid Commun* 21:1032–1034
- Şen M, Hayrabolu H (2012) Radiation synthesis and characterization of the network structure of natural/synthetic double-network superabsorbent polymers. *Radiat Phys Chem* 81:1378–1382
- Sawut A, Yimit M, Sun W, Nurulla I (2014) Photopolymerisation and characterization of maleylated cellulose-g-poly(acrylic acid) superabsorbent polymer. *Carbohydr Polym* 101:231–239
- Gao JZ, Wang AX, Li Y, Fu Y, Wu JL, Wang YD, Wang YJ (2008) Synthesis and characterization of superabsorbent composite by using glow discharge electrolysis plasma. *React Funct Polym* 68: 1377–1383
- Gao JZ, Ma DL, Lu QF, Li Y, Li XF, Yang W (2010) Synthesis and characterization of montmorillonite-graft-acrylic acid

- superabsorbent by using glow-discharge electrolysis plasma. *Plasma Chem Plasma Process* 30:873–883
15. Wang XY, Zhou MH, Jin XL (2012) Application of glow discharge plasma for wastewater treatment. *Electrochim Acta* 83:501–512
  16. Harada K, Iwasaki T (1977) Syntheses of amino acids from aliphatic carboxylic acid by glow discharge electrolysis. *Nature* 250:426–428
  17. Harada K, Suzuki S (1977) Formation of amino acids from elemental carbon by glow discharge electrolysis. *Nature* 266:275–276
  18. Malik MA, Ghaffar A, Malik SA (2001) Water purification by electrical discharges. *Plasma Sources Sci Technol* 10:82–91
  19. Tezuka M, Iwasaki M (1998) Plasma induced degradation of chlorophenols in an aqueous solution. *Thin Solid Films* 316:123–127
  20. Lu QF, Yu J, Gao JZ (2006) Degradation of 2,4-dichlorophenol by using glow discharge electrolysis. *J Hazard Mater* 136:526–531
  21. Friedrich JF, Mix R, Schulze RD (2008) New plasma techniques for polymer surface modification with monotype functional groups. *Plasma Process Polym* 5:407–423
  22. Djowe AT, Laminsi S, Njopwouo D, Acayanka E, Gaigneaux EM (2013) Surface modification of smectite clay induced by nonthermal gliding arc plasma at atmospheric pressure. *Plasma Chem Plasma Process* 33:707–723
  23. Lu QF, Yu J, Gao JZ, Yang W, Li Y (2011) Glow-discharge electrolysis plasma induced synthesis of polyvinylpyrrolidone/acrylic acid hydrogel and its adsorption properties for heavy-metal ions. *Plasma Process Polym* 8:803–814
  24. Yu J, Pan YP, Lu QF, Yang W, Gao JZ, Li Y (2013) Synthesis and swelling behaviors of P(AMPS-co-AAc) superabsorbent hydrogel produced by glow-discharge electrolysis plasma. *Plasma Chem Plasma Process* 33:219–235
  25. Neaman A, Singer A (2004) Possible use of the Sacalum (Yucatan) palygorskite as drilling muds. *Appl Clay Sci* 25:121–124
  26. Yadav M, Rhee KY (2012) Superabsorbent nanocomposite (alginate-g-PAMPS/MMT): synthesis, characterization and swelling behavior. *Carbohydr Polym* 90:165–173
  27. Abd El-Mohdy HL (2013) Radiation initiated synthesis of 2-acrylamidoglycolic acid grafted carboxymethyl cellulose as pH-sensitive hydrogel. *Polymer Engineering Science* 54:2753–2761
  28. Joshi AA, Locke BR, Arce P, Finney WC (1995) Formation of hydroxyl radicals, hydrogen peroxide and aqueous electrons by pulsed streamer corona discharge in aqueous solution. *J Hazard Mater* 41:3–30
  29. Hickling A, Ingram MD (1964) Glow-discharge electrolysis. *J Electroanal Chem* 8:65–81
  30. Sengupta SK, Singh R, Srivastva AK (1998) A study on the nonfaradaic yields of anodic contact glow discharge electrolysis using cerous ion as the scavenger: an estimate of the primary yield of OH radicals. *Indian J Chem A* 37:558–560
  31. Sun B, Sato M, Clements JS (1997) Optical study of active species produced by a pulsed streamer corona discharge in water. *J Electroanal Chem* 39:189–202
  32. Brisset JL, Moussa D, Doubla A, Hnatiuc E, Hnatiuc B, Youbi GK, Herry JM, Naïtali M, Bellon-Fontaine MN (2008) Chemical reactivity of discharges and temporal post-discharges in plasma treatment of aqueous media: examples of gliding discharge treated solutions. *Ind Eng Chem Res* 47:5761–5781
  33. Malik MA, Ahmed M, Rehman E, Naheed R, Ghaffar A (2003) Synthesis of superabsorbent copolymers by pulsed corona discharges in water. *Plasma Polym* 8:271–279
  34. Chisholm JE (1992) Powder diffraction patterns and structural models for palygorskite. *Can Mineral* 30:61–73
  35. Lei XP, Liu YS, Su ZX (2008) Synthesis and characterization of organo-attapulgit/polyaniline-dodecylbenzenesulfonic acid based on emulsion polymerization method. *Polym Compos* 29:239–244
  36. Zhang JP, Wang Q, Wang AQ (2007) Synthesis and characterization of chitosan-g-poly(acrylic acid)/attapulgit superabsorbent composites. *Carbohydr Polym* 68:367–374
  37. Limpanyoon N, Seetapan N, Kiatkamjornwong S (2011) Acrylamide/2-acrylamido-2-methylpropane sulfonic acid and associated sodium salt superabsorbent copolymer nanocomposites with mica as fire retardants. *Polym Degrad Stabil* 96:1054–1063
  38. Bao Y, Ma JZ, Li N (2011) Synthesis and swelling behaviors of sodium carboxymethyl cellulose-g-poly(AA-co-AM-co-AMPS)/MMT superabsorbent hydrogel. *Carbohydr Polym* 84:76–82
  39. Peng ZQ, Chen DJ (2006) Alignment effect of attapulgit on the mechanical properties of poly(vinyl alcohol)/attapulgit nanocomposite fibers. *J Polym Sci B Polym Phys* 44:1995–2000
  40. Li A, Wang AQ (2005) Synthesis and properties of clay-based superabsorbent composite. *Eur Polym J* 41:1630–1637
  41. Karadag E, Uzum OB, Saraydin D (2005) Water uptake in chemically crosslinked poly(acrylamide-co-crotonic acid) hydrogels. *Mater Des* 26:265–270
  42. Spagnol C, Rodrigues FHA, Pereira AGB, Fajardo AR, Rubira AF, Muniz EC (2012) Superabsorbent hydrogel composite made of cellulose nanofibrils and chitosan-graft-poly(acrylic acid). *Carbohydr Polym* 87:2038–2045
  43. Pourjavadi A, Barzegar S, Zeidabadi F (2007) Synthesis and properties of biodegradable hydrogels of  $\kappa$ -carrageenan grafted acrylic acid-co-2-acrylamido-2-methylpropanesulfonic acid as candidates for drug delivery systems. *React Funct Polym* 67:644–654
  44. Spagnol C, Rodrigues FHA, Neto AGVC, Pereira AGB, Fajardo AR, Radovanovic E, Rubira AF, Muniz EC (2012) Nanocomposites based on poly(acrylamide-co-acrylate) and cellulose nanowhiskers. *Eur Polym J* 48:454–463
  45. Lu QF, Yu J, Gao JZ, Yang W, Li Y (2012) A promising absorbent of acrylic acid/poly(ethylene glycol) hydrogel prepared by glow-discharge electrolysis plasma. *Cent Eur J Chem* 10:1349–1359
  46. Vimonses V, Lei SM, Jin B, Chow CWK, Saint C (2009) Kinetic study and equilibrium isotherm analysis of Congo red adsorption by clay materials. *Chem Eng J* 148:354–364
  47. Lorenc-Grabowska E, Gryglewicz G (2007) Adsorption characteristics of Congo red on coal-based mesoporous activated carbon. *Dyes Pigments* 74:34–40
  48. Barkakati P, Begum A, Das ML, Rao PG (2010) Adsorptive separation of ginsenoside from aqueous solution by polymeric resins: equilibrium, kinetic and thermodynamic studies. *Chem Eng J* 161:34–45
  49. Crini G (2008) Kinetic and equilibrium studies on the removal of cationic dyes from aqueous solution by adsorption onto a cyclodextrin polymer. *Dyes Pigments* 77:415–426
  50. Yu J, Yang GG, Pan YP, Lu QF, Yang W, Gao JZ (2014) Poly(acrylamide-co-acrylic acid) hydrogel induced by glow-discharge electrolysis plasma and its adsorption properties for cationic dyes. *Plasma Sci Technol* 16:767–776
  51. Reddy DHK, Lee SM (2013) Application of magnetic chitosan composites for the removal of toxic metal and dyes from aqueous solutions. *Adv Colloid Interf Sci* 201-202:68–93
  52. Crini G, Peindy HN, Gimbert F, Robert C (2007) Removal of C.I. Basic green 4 (malachite green) from aqueous solutions by adsorption using cyclodextrin-based adsorbent: kinetic and equilibrium studies. *Sep Purif Technol* 53:97–110
  53. Wong YC, Szeto YS, Cheung WH, McKay G (2004) Adsorption of acid dyes on chitosan-equilibrium isotherm analyses. *Process Biochem* 39:693–702